Construction of a hybrid lung model by combining a real geometry of the upper airways and an idealized geometry of the lower airways

R. Agujetas[1], R. Barrio-Perotti[2], C. Ferrera[3], A. Pandal-Blanco[4], D. K. Walters[5] and A. Fernández-Tena[6]

[1] Departamento de Ingeniería Mecánica, Energética y de los Materiales and ICCAEx, Universidad de Extremadura, Spain, e-mail rao@unex.es.
[2] Departamento de Energía, Universidad de Oviedo and GRUBIPU-ISPA, Spain, e-mail barrioraul@uniovi.es.
[3] Departamento de Ingeniería Mecánica, Energética y de los Materiales and ICCAEx, Universidad de Extremadura, Spain, e-mail cfll@unex.es.
[4] Departamento de Energía, Universidad de Oviedo and GRUBIPU-ISPA, Spain, e-mail pandaladrian@uniovi.es.
[5] School of Aerospace and Mechanical Engineering, University of Oklahoma, USA, e-mail d.keith.walters@ou.edu.
[6] Facultad de Enfermería, Universidad de Oviedo, Instituto Nacional de Silicosis and GRUBIPU-ISPA, Spain, e-mail tenaana@uniovi.es. Corresponding Author.

Abstract

- Background and Objective: Health care costs represent a substantial an increasing percentage of global expenditures. One key component is treatment of respiratory diseases, which account for one in twelve deaths in Europe. Computational simulations of lung airflow have potential to provide considerable cost reduction and improved outcomes. Such simulations require accurate in silico modelling of the lung airway. The geometry of the lung is extremely complex and for this reason very simple morphologies have primarily been used to date. The objective of this work is to develop an effective methodology for the creation of hybrid pulmonary geometries combining patient-specific models obtained from CT images and idealized pulmonary models, for the purpose of carrying out experimental and numerical studies on aerosol/particle transport and deposition in inhaled drug delivery.
- Methods: For the construction of the hybrid numerical model, lung images obtained from computed tomography were exported to the DICOM format to be treated with a commercial software to build the patient-specific part of the model. At the distal terminus of each airway of this portion of the model, an idealization of a single airway path is connected, extending to the sixteenth generation. Because these two parts have different endings, it is necessary to create an intermediate solid to link them together. Physically realistic treatment of truncated airway boundaries in the model was accomplished by mapping of the flow velocity distribution from corresponding conducting airway segments.
- Results: The model was verified using two sets of simulations, steady inspiration/expiration and transient simulation of forced spirometry. The results showed that the hybrid model is capable of providing a realistic description of air flow dynamics in the lung while substantially reducing computational costs relative to models of the full airway tree.
- Conclusions: The model development outlined here represents an important step toward computational simulation of lung dynamics for patient-specific applications. Further

research work may consist of investigating specific diseases, such as chronic bronchitis and pulmonary emphysema, as well as the study of the deposition of pollutants or drugs in the airways.

Keywords: CFD; CT images; hybrid model of human airway; meshing optimization; virtual topology

1. Introduction

Health care costs rank near the top of global public and private expenditures and are expected to substantially increase in the European Union (EU) over the next few decades as a result of the aging of the population [1]. Of these expenses, the second largest is due to respiratory disease, which is responsible for one in twelve deaths in Europe [2, 3]. This is exacerbated by inhalation of harmful particles, including tobacco smoke, mainly in urban environments. Researchers are therefore interested in better understanding the underlying flow and particle transport in the human lung airway in order to more effectively address care and prevention of respiratory disease, including effective dosing of inhaled medicinal interventions.

The most widely used experimental technique for the study of the respiratory system is spirometry, which measures pulmonary flow via the mouth but does not provide information on its behaviour in the bronchial tree [4]. Therefore, problem areas cannot be directly evaluated and it is not known if medical treatments successfully reach the damaged tissues and if they do so in the right amounts [5]. For this reason, the European Lung Foundation (ELF), the Food and Drug Administration (US FDA) and the pharmaceutical industry have shown an increasing interest in the development of studies for the controlled deposition of inhaled drugs [6, 7], which can help to maximize treatment efficiency and minimize secondary effects of inhaled drugs. To achieve this objective, it is necessary not only to develop patient-specific treatments [8], but also to understand the detailed underlying flow dynamics in the lung. Bioengineering research may therefore provide crucial information, with in-vivo [9-12] and in-vitro [13-17] studies. Nevertheless, the resolution of the different imaging techniques is not accurate enough to quantify the deposition in specific locations, consequently, in-silico simulations provide the vast majority of the reported information [15]. These simulations can facilitate personalized treatment plans, development of new drugs, design of new delivery devices, and potentially may lead to entirely new treatment techniques [18]. In addition, such simulations may reduce the cost of introducing new products by as much as 90% by the year 2025 [18, 19].

Applied computational fluid dynamics (CFD) simulations to study the behaviour of the respiratory system are generally performed in two phases: the generation and mesh of a computational flow domain based on a given anatomical model, and numerical resolution of the hydrodynamic equations for that geometry under a specified set of respiratory conditions. The information obtained is highly detailed and is available in an increasingly shorter time due to the steady increase in the computing speed, capacity and amount of computational resources. CFD allows precise calculation of parameters such as air velocity, pressure, temperature, humidity, and particle distribution that are difficult to estimate using alternative

techniques. However, even more important is the fact that CFD allows the study of problems that have no analytical solution and cannot be tested experimentally [20], providing researchers with an invaluable tool. Additionally, thanks to the CFD techniques, it is possible to test and compare several different treatment options in patients before and after a surgical intervention [21, 22]. In theory, it can even predict the outcome of a real intervention by first performing a virtual intervention [8].

The geometry of the lung is extremely complex and for this reason very simple morphological models have primarily been used for generalized analysis in prior studies. Phalen and Raabe [23] indicate that the first documented mathematical model used for particle deposition analysis was due to Findeisen, which disregarded the region of the airway located between the oronasal opening and the trachea, and assumed only 9 generations of dichotomous branching structure between the trachea and the alveolar sacs. They also indicate that Landahl added nose, mouth, pharynx and additional alveolar ducts to this model. Later, Davies [24] further enhanced it by adding more anatomical details starting from the mouth and reaching the alveolar sacs in the 15^{th} generation. The actual 23^{th} generations was not reached until Weibel [25] proposed a complete anatomical model of the airway branching structure, the most cited in the scientific literature. Starting from the trachea (generation 0), it assumes that the airways in the same generation are cylinders of constant diameter, each dividing successively into two symmetrical branches (regular dichotomy) until reaching the alveolar sacs. To this symmetric model, Horsfield and Cumming [26] introduced asymmetries in the diameter of the airways and the angles of the branches based on actual measurements of human airway morphology. As the level of available anatomical detail in morphological measurements increased, the accuracy in the models improved in the higher generations [5, 23]. None of the models described above accurately reproduce the distribution of airways in specific regions of the lung. Kitaoka et al. [27] proposed an algorithm to generate a 3D model of the bronchial tree based on a series of mathematical rules of the airways, which was followed by other researchers [5]. Many of these models are idealized, with the morphology obtained from models of corpses [28], yielding average values of airway diameters of the different generations, but not their patient-specific details. Even within the same person, the diameter of a given bronchus at specific generation is not uniform, but may vary significantly depending on the location.

As the generations included in a lung airway model increase, the model gets exponentially larger and more geometrically complex. For example, a model that fully resolves the airway up to the 16^{th} generation will have 65,536 (2^{16}) separate airway termini and 131,071 (2^{16+1}-1) individual airway branch segments. A CFD solution of flow in all branches with adequate numerical accuracy for clinical purposes would require a number of mesh elements (cells) on the order of several hundred million. Such a simulation is well beyond the capabilities of most current high-performance computing architectures, so some degree of model simplification remains necessary. Nowak et al. [29] divided the airway generations into subunits to simulate steady inhalation. In their approach, the inlet boundary condition for a given subunit was obtained from the outlet of the simulation in the immediately preceding (upstream) subunit. An alternative approach is to truncate the model by removing some amount of branching structure and applying appropriate boundary conditions on the distal termini of the truncated branches. Gemci et al. [30] used this approach for a truncated geometry that extended up to the 17^{th} generation, which only included 1,453 bronchi of the existing 131,071. They applied

a constant pressure as boundary condition in the truncated branches to simulate steady inhalation. Walters and Luke [31] used a statistical description based on a finite number of fully resolved flow paths in order to provide a detailed description of the entire flow field to simulate steady inhalation in the human airways up to the 12th generation. They proposed a technique to map pressures from equivalent locations in resolved airway branches onto the outlet boundaries of the truncated branches.

Although it is an ideal geometry, 3D CFD models have the advantage that they determine any fluid property, and particles too, in any position of any of the lung branches. In the hybrid model, since the first generations correspond to a real geometry, the distribution of the particles is also done in a real way, so that it is possible to know quite accurately the amount that goes to each lung lobe. The 1D models give a joint spatial distribution of the particle situation, without differentiating the lobe in which they are found, and they don't take into account the aerodynamics of the bifurcations and the impact of the particles in the pantaloons, the asymmetric velocity distribution in each section, etc.

Nevertheless, the main deficiency with those previous efforts making use of truncated airway geometries is that they only prescribed boundary conditions for the truncated airway branches that allowed simulation of inhalation only. This problem was addressed in the study of Fernández-Tena et al. [32, 33], where a model up to the 16th generation was used being able to work on both, inspiration and expiration movements truncating one of the two branches downstream of each bifurcation, beginning at the first generation. To address the fact that velocity in a given airway cross section is not uniform, a method was proposed to perform cell-to-cell velocity mapping from resolved branches to truncated boundaries. This model was validated by comparison with forced spirometry experiments and has been further assessed in more recent works, including also particle deposition [34, 35], providing really accurate results with low relative error.

Despite all these efforts for simplification, nowadays research work should make a bigger difference and hence, investigations must be directed towards patient specific treatment. In order to reach this goal, real patient characteristics should be retained and thus, the use of lung models reconstructed from images obtained by magnetic resonance (MRI) or computed tomography (CT) can be the winning approach for a great clinical tool [10, 26, 36]. Reference models containing airways up to the 17th generation have been constructed employing High Resolution CT (HRCT) to rubber casts obtained from corpses [37]. The problem of these techniques is the limited extent of valid data which makes impossible to simulate a complete lung. Cebral and Summers [38] managed to reconstruct up to the 4th generation, verifying that the diameter and length of the branches decrease from generation to generation. The use of segmentation techniques allowed Nakamura et al. [39] to estimate morphological data up to the 14th generation, although the obtained values of airway diameters were only found to be valid up to the 4th generation when compared with measurements in corpses. They indicate that the method is potentially accurate up to the 8th generation, but the values would have to be corrected with an adjustment curve between measured diameters and average values of the grey threshold used in the segmentation [40]. In smaller branches, the authors show a clear dispersion of the segmented diameters and indicate that the extracted lumen is overestimated. In recent years, 6th [10, 41, 42] and 7th [43] generations are consistently retrieved. Depending on the subject, specifically in those whose airways are larger, branches

of the 9th [44], 10th [45], 11th [46] or even 15th [16] may have been captured. Nevertheless, anatomic measurements over the 16th generation are difficult to achieve with the actual imaging techniques [15] and the same authors claim that bronchus below 5 mm cannot be resolved with the latest CT technology. Other authors reduce this limit to 0.6 mm with HRCT or MRI techniques, indicating that the details of this measurement can also be smoothed out during image processing [47]. Different simulations have proved that smaller particles surpass the 17th generation [48].

For all the reasons discussed, CT-based models need to be completed with airway generation algorithms in order to model the entire lung [45, 49, 50]. Resistance models have also been employed [51]. Tawhai et al. [52] generated a curvilinear tubular model up to the 10th generation from CT data consistent with published anatomical measurements. However, it is crucial to retain the particular geometrical details of a patient, as proven in other fields [53]. Geometry reconstruction programs based on CT images generate designs and meshes that are not necessarily optimal for CFD simulations. To overcome these disadvantages, Fernández-Tena et al. [54] have proposed a method that improves the quality of geometric models combining a virtual topology with the patch-independent mesh algorithm using a commercial package [55].

Since the authors themselves already have contrasting models, a real one coming from CT images and another ideal one based on the one designed by Weibel, as well as procedures incorporating the effects of truncated branches, and for calculating the time step in transient processes as a function of dependent variables, the objective of this work is to develop an effective methodology for the creation of hybrid pulmonary geometries using a combination of patient-specific models obtained from computed tomography (CT) images and idealized pulmonary models, reaching the entire conductive zone. The purpose of the hybrid pulmonary geometries is to carry out experimental and numerical studies on aerosol/particle transport and deposition in inhaled drug delivery. These hybrid geometries retain most of the patient-specific features and a complete lung simulation can be performed without additional computational cost.

2. Methods

For the construction of the model geometry, it is necessary to treat the lung images obtained from computed tomography, which are exported to the DICOM (Digital Image and Communication in Medicine) format. The available resolution of the DICOM images is 512 x 512 pixels, where 680 μm is the size of each pixel, with a gray intensity value according to the scale of Hounsfield [56]. As it is known that there is a direct relationship between the density of each anatomical structure and the gray value assigned to each pixel in the image, the 3D Slicer software [57] was used to group similar gray values, identifying the threshold between the different tissues. In this case, a pixel mask was defined in the region of interest with a threshold range of 190-250 to extract the lung tree [58]. From the created dynamic region, the 3D model was implemented and a design tool, which optimizes the surface of the model by means of adjustment and smoothing processes, used to prepare it for the numerical simulations (Figure 1). Any small deviation between the original geometry and the resulting

model is not expected to significantly affect the flow simulation results.

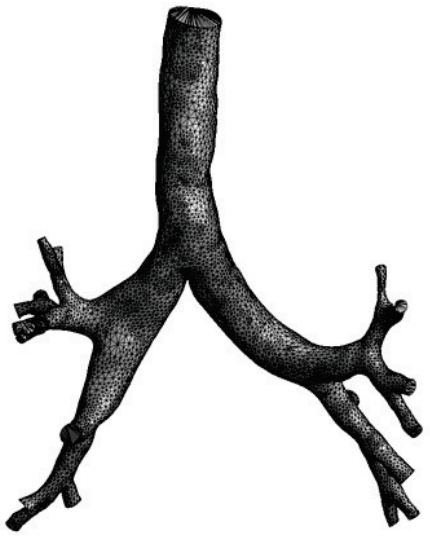

Figure 1. Model obtained from CT images after import into ANSYS DesignModeler. Final branches are obtained until the generations between the 3rd and 5th.

In this case, since the maximum generation to which all branches reach is the third, it was decided to truncate the patient-specific geometry at this point and reproduce the remaining generations using the idealized model of pulmonary geometry. Although the tomography images might have a higher resolution and other generations can be reached (fourth, fifth, etc.), the model reconstruction procedure is the same. To remove the branches that exceed the 3rd generation, the "Slice" tool is used, which separates a solid in two from a plane (Figure 2). This same method can be used to separate generations so that the CFD simulation results can be used to study particle deposition.

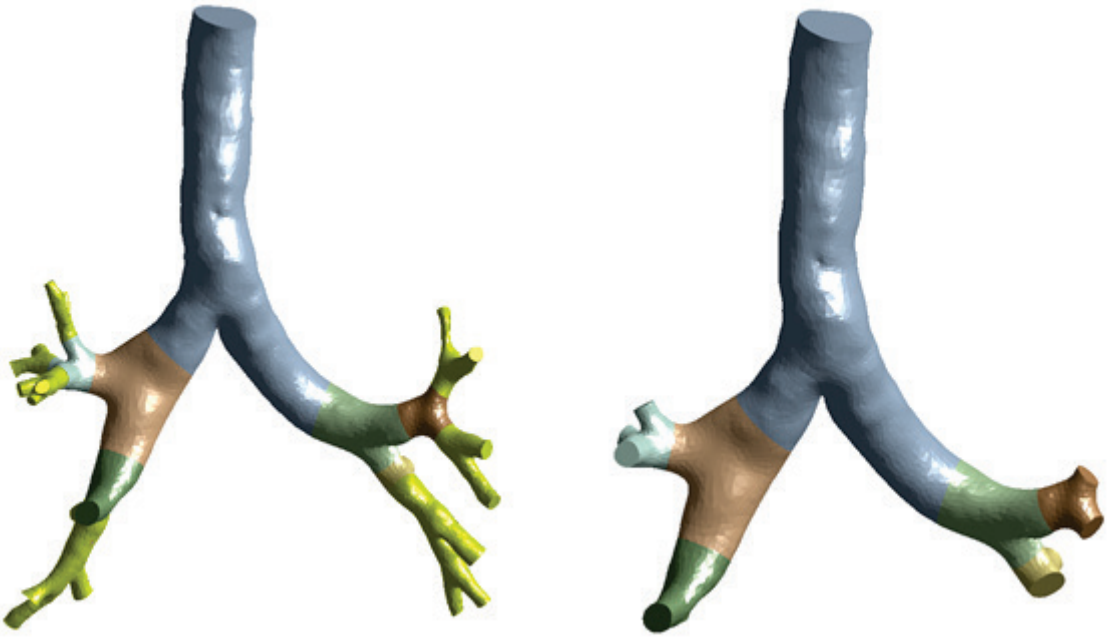

Figure 2. Numerical model from CT (left) and after cutting the branches posterior to the 3rd generation, divided into solids by generations.

Once the CT model has been truncated at the 3rd generation, the terminal surfaces have different shapes and sizes that depend on their position and orientation and on the morphology of the lung. It is intended to place in each truncated branch an extension of the parametric lung that includes only a single pathway through the remaining generations, following the strategy employed by Walters [31] and Fernández-Tena [32, 33]. According to this model, the number of discrete pathways in the overall lung model is equal to the termini of the CT-based portion of the model depicted in Figure 2. It is apparent from the figure that in this case there are 9 pathways to be added to the CT-based model. These pathways follow the Weibel model (Figure 3a), whose construction is documented in previous works by the authors [32-35]. The straight sections of the ideal part are made up of cylinders, and branches in equivalent generations are assumed to be geometrically identical. Since the terminal branches of the CT-based portion part have endings with non-circular shapes and differing sizes (Figure 3b), to connect the two portions with the ideal part it is necessary to model a solid that makes the adaptation between both shapes, as illustrated in Figure 3c. This solid starts from an irregular shape at each terminus of the CT-based model and ends in a circular shape which matches the most proximal surface of the idealized model, as illustrated in Figure 3d. This is done ending the real part in a surface perpendicular to its axis, positioning the ideal part along the same axis, at a distance of about half a diameter, and generating a connecting geometry with a lateral surface resting on the perimeter of the real surface and the circle of the beginning of the idealized geometry. In this way, the hybrid model is achieved, reaching the sixteenth generation with a single idealized pathway from each branch of the third generation of the patient specific CT-based model. The complete model is shown in Figure 4. It should be noted that a complete model of the bronchopulmonary airway tree up to 16th generation would necessarily include 65,536 (2^{16}) ends and 131,071 (2^{16+1}-1) individual airway

branch segments. In contrast, this hybrid model, showed in Figure 4, contains only 9 ends and 132 (9*[16-4+1] + [2^{3+1}-1]) individual airway branch segments. Therefore, the overall reduction in computational expense for CFD simulation is estimated to be ~99.9% (132/131,071).

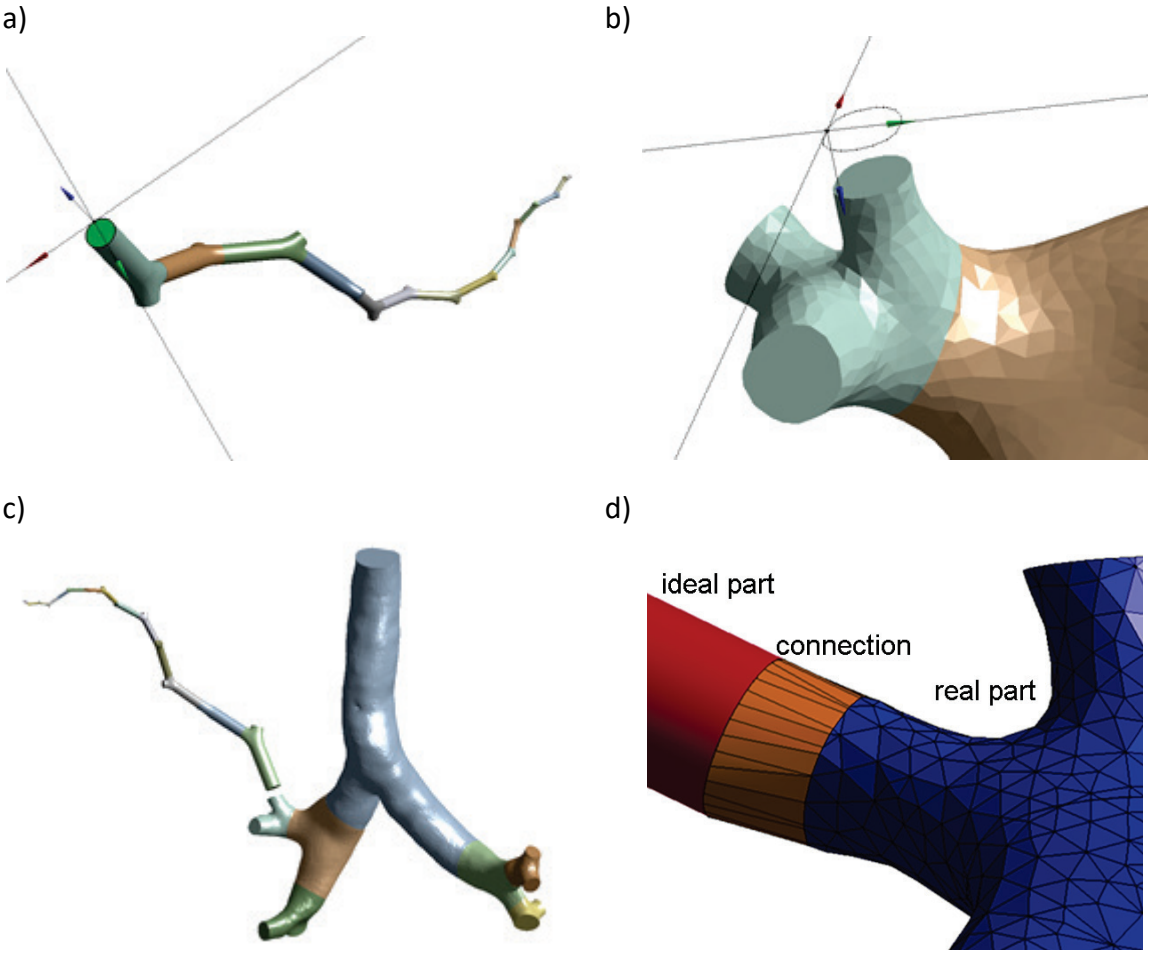

Figure 3: a) extension of the ideal lung; b) end of a truncated branch of the CT model; c) offset of the ideal model due to non-coincidence of the previous surfaces; d) solid obtained from the connection between polygon and circumference, with detail of the three resulting solids (ideal part, connection and CT part).

Once the model has been completed, it is necessary to generate a computational mesh that can be used for CFD simulation. Due to the way in which the CT model is obtained, there is an arbitrarily tessellated surface (Figure 5) that can make it difficult to define the surface mesh in the upper region. In order to improve the quality of the mesh and reduce the time it takes to generate the mesh and the subsequent calculations, a three-dimensional geometry was made using a virtual topology complemented by a patch-independent mesh algorithm, via a method documented in a previous work by the authors [54].

Figure 4. Lung model up to the 16th generation, blue color part obtained from CT, yellow color ideal part.

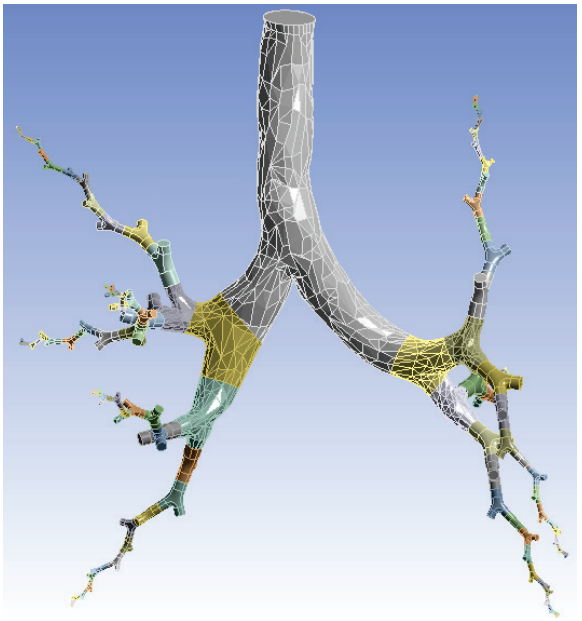

Figure 5. Lung model with tessellated surface

It is desired to have approximately the same number of cells and a similar level of near-wall mesh resolution within each generation. In the current work, the three-dimensional geometry was meshed using the commercial code ANSYS [55]. The mesh consisted of tetrahedral cells in the inner region of each airway branch, and five layers of triangular prisms near the airway wall. An unstructured topology was chosen because it allows easier adaptation of the mesh to complex geometries. The prismatic layers are necessary to effectively resolve steep velocity gradients in the near-wall boundary layer. The dimensionless wall distance (y+) for the cells in the first prismatic layer of the wall was estimated to be less than one, indicating that the centers of the cells next to the wall are well inside the laminar sublayer [20]. This was subsequently verified during post-processing of the simulations. The resulting mesh topology is illustrated in Figure 6.

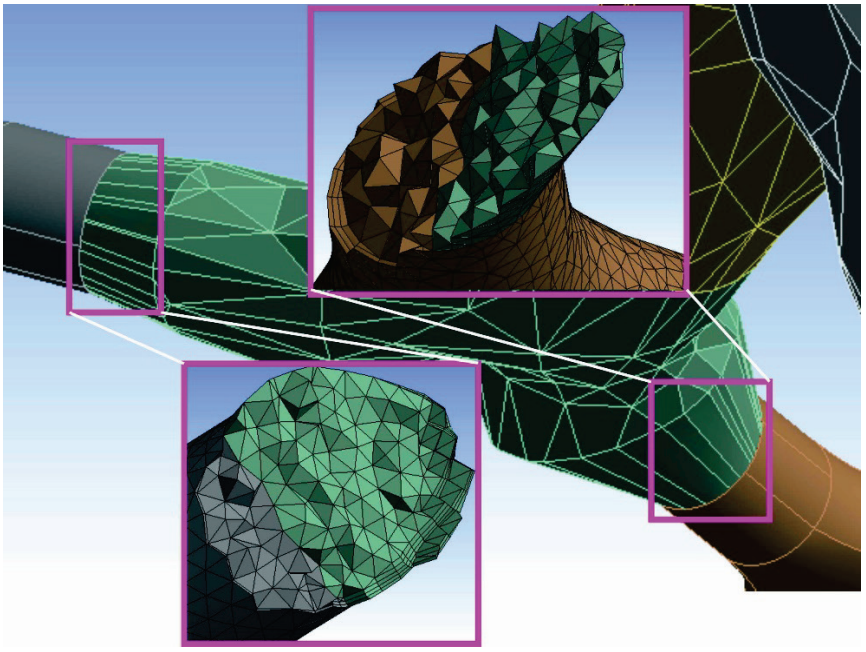

Figure 6. Lung model up to the 16th generation, grey color mesh is the part obtained from CT, green color bets to the adaptation solid and brown color is the parametric part. It can be observed the mesh, with tetrahedral cells and five inflation layers over the walls.

The total number of cells in the baseline mesh was approximately $3.16x10^6$, with a range of cell volume sizes between $4.46x10^{-15}$ m^3 and $2.46x10^{-10}$ m^3. An analysis of the quality of the mesh yielded a satisfactory result, indicating a magnitude of the equisized skew that was below 0.7 for 98% of the cells in the mesh. To assess the effect of mesh resolution and verify grid independence of the results, five coarser and finer grids of size $0.50x10^6$,$2.45x10^6$, $4.12x10^6$, $5.10x10^6$ and $9.12x10^6$ cells were built in addition to the baseline mesh. Simulations were carried out by imposing a constant flow rate at the lung inlet, using as a variable of reference the static pressure drop between the inlet and the outlet, which quantifies the overall resistance flow in the lung airway. It was observed (Figure 7) that the results on the four most refined grids differed by less than 1.9%, and the result on the coarsest mesh differed by 12.3% and 5.2% from that on the finest mesh. Therefore, it was concluded that the baseline mesh with $3.16x10^6$ cells was sufficiently accurate and represented the optimum choice in terms of computational expense since the required calculation time is significantly shorter. As a result, it was selected for the following simulations.

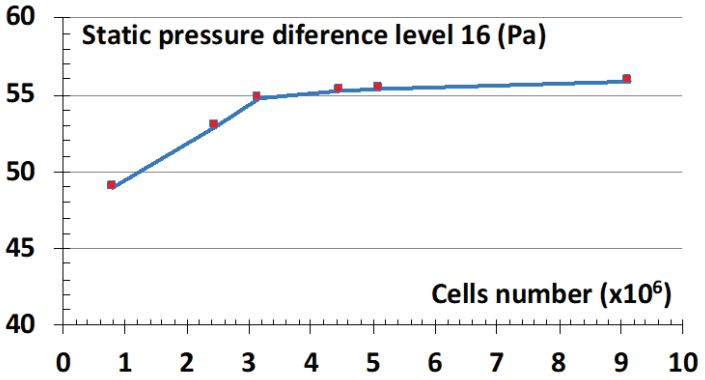

Figure 7. Results of the mesh independence test.

This hybrid geometry model was evaluated in similar way to previous works of the authors [32-35], using steady and transient flow in the lung airway. The presence of truncated boundaries at generations 4-15 require specialized boundary conditions since the pressure and/or velocity distribution is not known at these locations. The boundary condition must nevertheless faithfully represent the effect of the removed airways on the flow in the remaining airways. It is known that in any straight tube with constant or quasi-constant non-zero mass flow, the velocity is not uniform, but varies radially with the velocity magnitude being greatest near the center and zero at the tube walls. For cases in which the flow is turned, there will also arise asymmetric flow distributions and secondary flow patterns including vortices. In order to retain this complexity in the reduced geometry model, the basis of the current approach is to map flow variables exactly from a region of the resolved mesh pathway to the unresolved truncated boundaries. In the present study, a user-defined function (UDF) developed by the authors was used [32-35]. The effect of the function is to copy the velocity vector of each of the mesh faces of the associated interior face to the corresponding mesh face in its symmetrical truncated branch. The effectiveness of this approach is demonstrated via validation CFD simulations.

The commercial code Ansys FLUENT [55] was used to solve the unsteady Reynolds-Averaged Navier-Stokes (URANS) equations [59]. The particular solver used was pressure-based and implicit since the flow is assumed to be well within the incompressible regime. Second-order discretization was used for the spatial and temporal derivatives in the governing equations. The SIMPLEC algorithm was used to solve the coupling between pressure and velocity fields. It is assumed that the flow in the lung airway may be laminar and/or turbulent within a single breathing cycle, therefore a turbulence model was used in the present simulations. Because it has shown previous success for simulation of complex non-stationary turbulent flows, the turbulence model chosen was the SST (Shear Stress Transport) k-ω model, which has proved to be the most efficient one under a RANS approach for both inhalation and exhalation [6, 15, 32, 60-63]. This model approximates a blended form of the standard k-ε and k-ω models. Inlet boundary conditions for the turbulence variables were intensity (5%) and viscosity ratio (10). Koullapis et al. [15], in an upper airway model, discuss the behavior of various LES and RANS turbulence models in the particle deposition. They indicate that with LES models more defined results can be obtained than with RANS, but it is necessary to use a number of cells one order

of magnitude larger, with a time step one order of magnitude smaller, which means using more powerful computers.

For unsteady flow cases, the time-step size was chosen to provide specified maximum value of the Courant-Friedrichs-Lewy (CFL) number during the entire flow cycle. Here the CFL number was defined as the ratio between the time interval and the residence time in a computational cell (CFL=vΔt/Δx), where "v" is the velocity magnitude in the cell, "Δt" is the time step size, and "Δx" is the characteristic size of the cell. To ensure accurate and computationally efficient simulation, a variable time-step method previously developed by the authors [32, 63] was implemented. The method adjusts the time-step size based on the instantaneous flow rate to ensure that the CFL number is approximately maintained throughout the simulation. Compared to a fixed time-step size, the method was found to reduce the required number of iterations. For example, if with a constant time step of 0.005 s for a forced spirometry of 7.77 s, 1,422 steps are necessary, following the described procedure, with a velocity range between 38.02 and -30.77 m/s, if velocity increments of 0.1 m/s are taken, 688 steps will be required, 52% less. The advantage of this method is that the whole range of the velocity dependent variable will be covered with absolute fidelity, gaining convergence security and computational time.

3. Results

Two test cases were selected for validation of the hybrid lung airway modelling methodology outlined above. The first test case is stationary flow with a specified flow rate. Both inhalation and exhalation are evaluated. The objective of this case was to verify the correct coupling of the two portions of the model geometry as well as the correct implementation of the boundary condition method for use in the truncated airway branches. The second test case was a forced spirometry simulation, encompassing both inspiration and expiration. The objective was to demonstrate model performance under more realistic respiratory conditions and to verify consistency of the model and boundary condition implementation.

For the first test based in steady inspiration and expiration, a specified volumetric flow rate of 65 L/min was applied as the boundary condition at the tracheal opening (generation 0). The boundary condition in the distal airway branches (16^{th} generation) was constant and uniform static (inspiration) or total (expiration) pressure. The boundary condition at truncated airway branches was applied based on the flow in the corresponding symmetric conducting branch, as described above. Figures 8 and 9 show pressure contours in inspiration and expiration, respectively, and Figures 10 and 11 show the velocity vectors at the outlets of truncated branches and their symmetrical counterparts in the corresponding conductive branches.

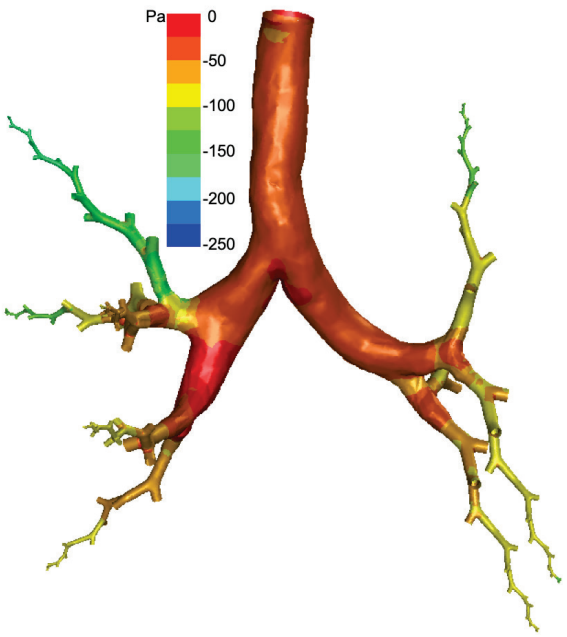

Figure 8. Pressure contours for a flow rate of 65 L/min in inspiration.

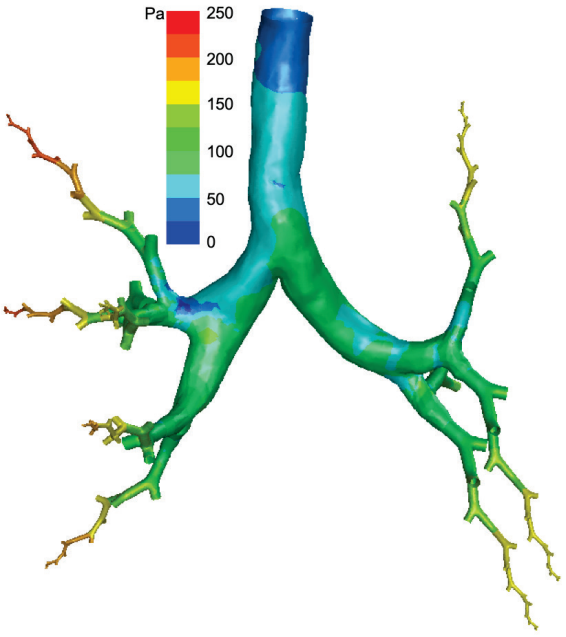

Figure 9. Pressure contours for a flow rate of 65 L/min in expiration.

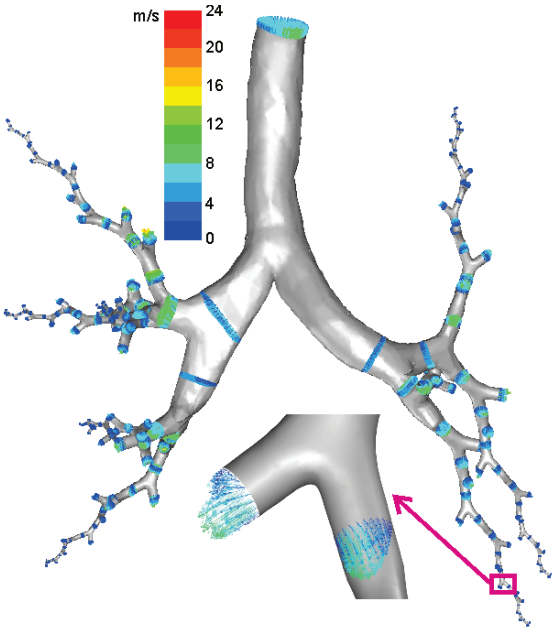

Figure 10. Velocity vectors for a flow rate of 65 L/min in inspiration.

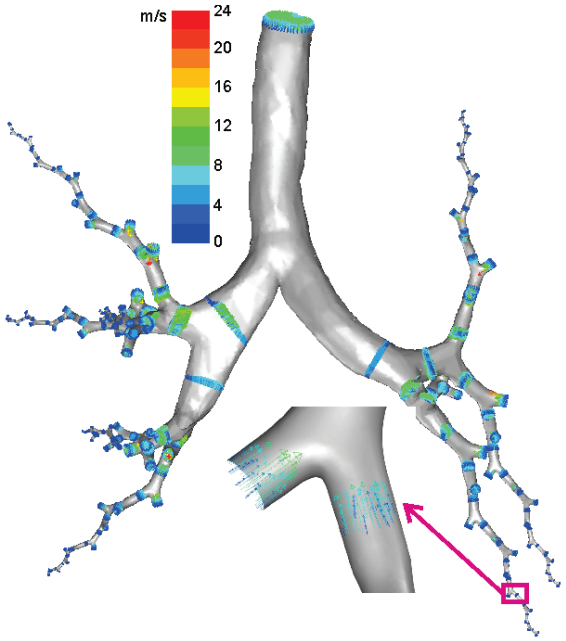

Figure 11. Velocity vectors for a flow rate of 65 L/min in expiration.

The second test is based on applying a transient condition, being the forced spirometry the only non-intrusive test available to pulmonologists to check lung function. This test consists of

measuring the flow of air that a patient inhales and exhales in a given time, presenting a high range of velocities with quick changes in flow rate during the inhalation-exhalation cycle. The representation of the flowrate and volume measurements obtained in a given time allows the pulmonologists to check the condition of the lungs. Therefore, the only way to check if the numerical model works well is to simulate the forced spirometry. This test will be done in two steps. In the first step, the simulation is carried out using the velocity (or flow rate) at the mouth, which is measured with the spirometer, as a limit condition. These simulation results allow us to know the values of all the variables in the numerical model, among them, the pressure in the distal zone, which is what causes the inlet and outlet of air from the lungs. A new simulation is then carried out in the second step, using the pressure in that distal zone as boundary condition. The model will work well if it can reproduce the flow at the outlet, which is what is to be compared with forced spirometry.

Spirometric data were obtained by means of a spirometer model CPFS/D USB, with a MedGraphics preVentTM pneumotachometer and BREEZESUITETM diagnostic software (Medical Graphics Corporation 2004, 350 OakGrove Parkway, St. Paul, Minnesota 55127-8599). Data was sampled every 0.005 seconds. Figure 12 shows the relationship between flow rate and lung volume versus time. It can be seen that after three normal breathing cycles, the portion corresponding to the manoeuvre of the forced spirometry itself corresponds to the data obtained between 11.31 and 19.08 seconds. To reproduce the same conditions computationally, the boundary conditions imposed in the model were the unsteady flow rate at generation 0 and either static or total pressure at 16th generation. The direction and magnitude of the flow rate was varied during the cycle using a user-defined function (UDF) implemented by the authors [32, 63] into the Ansys FLUENT solver.

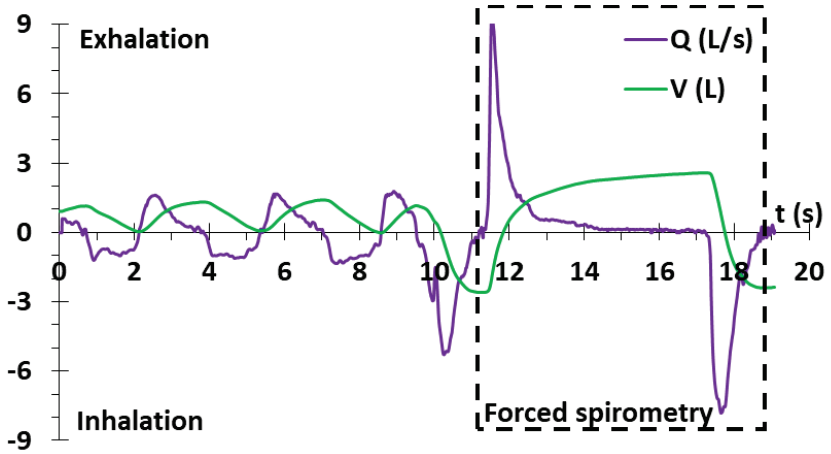

Figure 12. Relationship between flow rate versus time in a respiratory cycle.

To ensure that no initial transients impacted the computational results, simulations were repeated for a total of 5 spirometric cycles (3,440 steps), at which point it was verified that cycle-to-cycle variations in flow behavior were negligible. Each cycle has a physical runtime of 7.77 seconds, equivalent to the physical time for the experimental spirometric cycle. The total

computational run time was approximately 120 h on an AMD Ryzen Threadripper 1900X 3.80 GHz computer running in parallel with 8 cores . Figure 13 provides an illustration of the convergence of flow variables during the fifth cycle. It is apparent from the behavior of the residuals that the simulation is well converged at each time step.

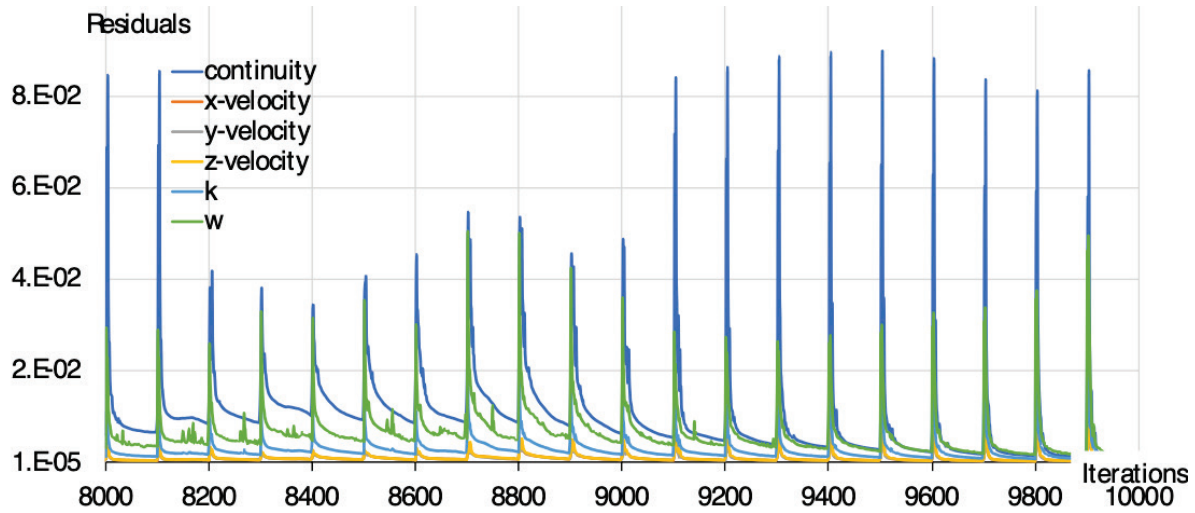

Figure 13. Convergence of the variables.

Figure 14 shows results obtained in this second simulation, in this case, the static pressure in the distal (16th) generation (average of all branches) and the volumetric flow rate used as boundary condition. There is a good agreement between both variables, when the pressure in the distal zone reaches the maximum and the minimum, the expiration and inspiration flows are also maximum and minimum.

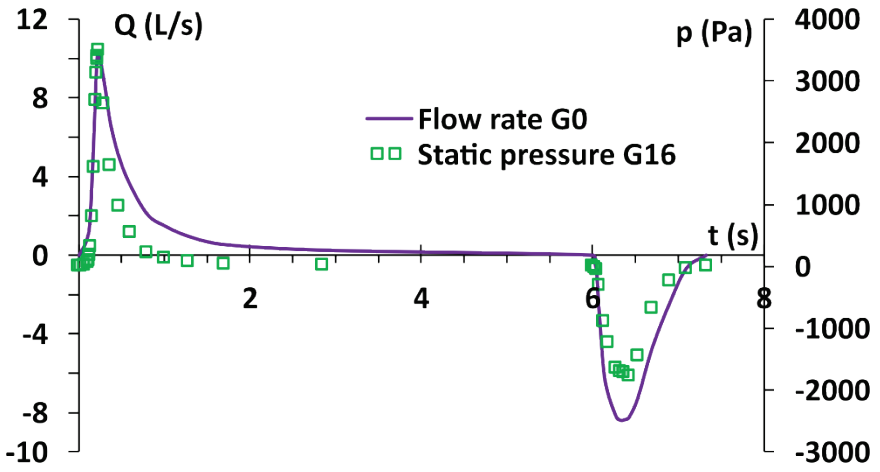

Figure 14. Numerical results obtained of the static pressure in the distal zone (16th generation) and experimental flowrate at the generation 0.

Once the behavior of the entire fluid field of the lung is known, a second spirometry simulation will be performed using a different boundary condition than in the first simulation. In this case, an unsteady total pressure (sum of static and dynamic pressure) condition was applied in the 16th generation, which was obtained from the first simulation. A constant static pressure was applied at generation 0. The conditions of the simulation are the same as those of the first one, carried out in the same equipment and with similar duration.

Figure 15 compares the numerical values of air velocity obtained at generation 0 with the experimental values obtained from the forced spirometry.

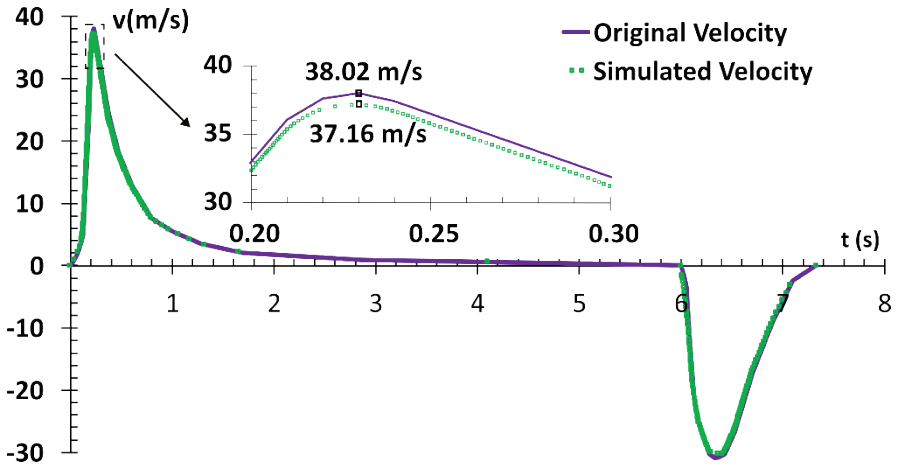

Figure 15. Comparison between the velocities obtained from forced spirometry and simulation at generation 0.

4. Discussion

The pressure contours shown in Figures 8 and 9, both in inspiration and expiration, depict that the flow adapts to the conditions of the pulmonary tree, distributing itself according to the resistance it finds in each of the branches, as in reality, with pressure losses in the direction of flow. In inspiration the maximum pressure occurs in the trachea and the minimum occurs in the most distal (16th) generation. In expiration the opposite occurs, the minimum pressure is in generation 0 while the maximum is in the 16th generation. Both are indicative of flow resistance in the lung airway. In the Figures 10 and 11, the velocity vectors at the outlet of truncated branches display physically realistic behavior, since they are exactly symmetrical to the velocity vectors at the corresponding location in the twin conducting airway downstream of the branching location. These results serve to demonstrate that the model behaves as intended.

For the unsteady spirometry simulations, it is significant that pressures and flowrates have similar time-dependent behavior at each generation during the spirometric cycle (Figure 14).

As shown in Figure 15, the results for velocity at generation 0 compare very closely with experimental results. The maximum velocity occurs at time 0.23 s, with predicted and experimental values of 37.16 and 38.01 m/s respectively. The discrepancy is less than 2.5%, which suggests that the method presented is capable of faithfully reproducing physiologically realistic results under realistic ventilation conditions. These results are in line with those shown by the same authors in previous works with this type of model [32-35].

5. Conclusions

A hybrid model of the human lung airway has been constructed using images obtained from computed tomography (CT) data to reproduce the trachea and upper airway region and an idealized morphology for the remainder of the geometry up to the 16^{th} generation. An intermediate solid model section is necessary to link the cylindrical sections of the idealized model to the non-cylindrical sections of the CT-based model. The lower airway region was constructed of a finite number of airway paths between the 6^{th} and 16^{th} generations. Boundary conditions for the truncated airways were specified by mapping the velocity distribution from the conducting airway downstream of a branch location to the corresponding truncated twin airway terminus.

The model performance was verified using two sets of simulations, corresponding to steady flow (inspiration and expiration) and to an unsteady forced spirometry. Results show that the hybrid model is capable of providing a realistic description of lung ventilation while reducing computational cost by approximately 99.9% compared to a complete model of the airway between generations 0 to 16.

The model development outlined here represents an important step toward computational simulation of lung dynamics for patient-specific applications. Further research work may consist of investigating specific diseases, such as chronic bronchitis and pulmonary emphysema, as well as the study of the deposition of pollutants or drugs in the airways.

Acknowledgements

This work was financially supported by the Spanish Ministry of Economy, Industry and Competitiveness - Instituto de Salud Carlos III under Project “Estudio de la influencia de la geometría de las vías respiratorias en las patologías pulmonares obstructivas (PI17/01639)”, Principado de Asturias under project “Ayudas a organismos públicos de investigación GRUPIN-IDI-2018-000205”, Junta de Extremadura under project “Ayudas para la realización de actividades de investigación y desarrollo tecnológico, de divulgación y de transferencia de conocimiento por los Grupos de Investigación de Extremadura (GR150014) and IB16119 (partially financed by FEDER)”, and Universidad de Oviedo under Project “Aprendizaje colaborativo orientado a la práctica de patologías: broncoscopias. PINN-17-A-045”.

Compliance with ethical standards

Conflicts of interest

The authors of the paper declare that they have no conflict of interest.

References

1. OECD and E. Union, *Health at a Glance: Europe 2018*. 2018.
2. EU, “Eurostat Statistics: Causes of death in the EU by type,” 2016. .
3. WHO, “The top 10 causes of death,” 2018.
4. Lange, P., Halpin, D. M., O’Donnell, D. E., & MacNee, W. (2016). Diagnosis, assessment, and phenotyping of COPD: beyond FEV1. *International journal of chronic obstructive pulmonary disease*, 11(Spec Iss), 3.
5. Ahookhosh, K., Pourmehran, O., Aminfar, H., Mohammadpourfard, M., Sarafraz, M. M., and Hamishehkar, H. (2020). “Development of human respiratory airway models: A review,” *Eur. J. Pharm. Sci.*, vol. 145, no. January, p. 105233.
6. Kolanjiyil, A. V., Kleinstreuer, C., Kleinstreuer, N. C., Pham, W., and Sadikot, R. T. (2019). “Mice-to-men comparison of inhaled drug-aerosol deposition and clearance,” *Respir. Physiol. Neurobiol.*, vol. 260, no. July 2018, pp. 82–94.
7. Lip Kwok, P. C. (2015). “Pharmaceutical aerosol electrostatics: a field with much potential for development,” *Ther. Deliv.*, vol. 6, no. 2, pp. 105–107, Feb.
8. Burrowes, K. S., De Backer, J., & Kumar, H. (2017). Image-based computational fluid dynamics in the lung: virtual reality or new clinical practice? *Wiley Interdisciplinary Reviews: Systems Biology and Medicine*, *9*(6), e1392.
9. P Longest, P. W., Tian, G., Khajeh-Hosseini-Dalasm, N., & Hindle, M. (2016). Validating whole-airway CFD predictions of DPI aerosol deposition at multiple flow rates. *Journal of aerosol medicine and pulmonary drug delivery*, *29*(6), 461-481.
10. Kang, W., Tawhai, M. H., Clark, A. R., Sá, R. C., Geier, E. T., Prisk, G. K., & Burrowes, K. S. (2018). In silico modeling of oxygen-enhanced MRI of specific ventilation. *Physiological reports*, *6*(7), e13659.
11. Addo, D. A., Kang, W., Prisk, G. K., Tawhai, M. H., & Burrowes, K. S. (2019). Optimizing human pulmonary perfusion measurement using an in silico model of arterial spin labeling magnetic resonance imaging. *Physiological reports*, *7*(11), e14077.
12. Bui, V. K. H., Moon, J. Y., Chae, M., Park, D., & Lee, Y. C. (2020). Prediction of Aerosol Deposition in the Human Respiratory Tract via Computational Models: A Review with Recent Updates. *Atmosphere*, *11*(2), 137.
13. Lizal, F., Elcner, J., Hopke, P. K., Jedelsky, J., & Jicha, M. (2012). Development of a realistic human airway model. *Proceedings of the Institution of Mechanical Engineers, Part H: Journal of Engineering in Medicine*, *226*(3), 197-207.
14. Lizal, F., Belka, M., Adam, J., Jedelsky, J., & Jicha, M. (2015). A method for in vitro regional aerosol deposition measurement in a model of the human tracheobronchial tree by the positron emission tomography. *Proceedings of the Institution of Mechanical Engineers, Part H: Journal of Engineering in Medicine*, *229*(10), 750-757.
15. Koullapis, P., Kassinos, S. C., Muela, J., Perez-Segarra, C., Rigola, J., Lehmkuhl, O., ... & Saveljic, I. (2018). Regional aerosol deposition in the human airways: The SimInhale

benchmark case and a critical assessment of in silico methods. *European Journal of Pharmaceutical Sciences*, *113*, 77-94.
16. Van de Moortele, T., Wendt, C. H., & Coletti, F. (2018). Morphological and functional properties of the conducting human airways investigated by in vivo computed tomography and in vitro MRI. *Journal of Applied Physiology*, *124*(2), 400-413.
17. Ahookhosh, K., Yaqoubi, S., Mohammadpourfard, M., Hamishehkar, H., & Aminfar, H. (2019). Experimental investigation of aerosol deposition through a realistic respiratory airway replica: An evaluation for MDI and DPI performance. *International journal of pharmaceutics*, *566*, 157-172.
18. Viceconti, M., Henney, A., & Morley-Fletcher, E. (2016). In silico clinical trials: how computer simulation will transform the biomedical industry. *International Journal of Clinical Trials*, *3*(2), 37-46.
19. Chiastra, C., Migliori, S., Burzotta, F., Dubini, G., & Migliavacca, F. (2018). Patient-specific modeling of stented coronary arteries reconstructed from optical coherence tomography: Towards a widespread clinical use of fluid dynamics analyses. *Journal of cardiovascular translational research*, *11*(2), 156-172.
20. Tu, C., Yeoh, J., Liu, G.-H. (2018). *Computational Fluid Dynamics*. Butterworth-Heinemann.
21. Vanhille, D. L., Garcia, G. J., Asan, O., Borojeni, A. A., Frank-Ito, D. O., Kimbell, J. S., ... & Rhee, J. S. (2018). Virtual surgery for the nasal airway: a preliminary report on decision support and technology acceptance. *JAMA facial plastic surgery*, *20*(1), 63-69.
22. Wofford, M. R., Kimbell, J. S., Frank, D. O., Dhandha, V., McKinney, K. A., Fleischman, G. M., ... & Senior, B. A. (2015). A computational study of functional endoscopic sinus surgery and maxillary sinus drug delivery. *Rhinology*, *53*(1), 41.
23. Phalen, R. F., & Raabe, O. G. (2016). The evolution of inhaled particle dose modeling: A review. *Journal of Aerosol Science*, *99*, 7-13.
24. Fernández Tena, A. and Casan Clarà, P. (2012) "Deposition of inhaled particles in the lungs," *Arch. Bronconeumol.*, vol. 48, no. 7, pp. 240–246.
25. Weibel, E. R. (1963). "Geometric and Dimensional Airway Models of Conductive, Transitory and Respiratory Zones of the Human Lung BT - Morphometry of the Human Lung," E. R. Weibel, Ed. Berlin, Heidelberg: Springer Berlin Heidelberg, pp. 136–142.
26. Verschakelen, J. A. and de Wever, W. (2018) *Computed Tomography of the Lung*. Springer-Verlag Berlin Heidelberg.
27. Kitaoka, H., Takaki, R., and Suki, B. (1999) "A three-dimensional model of the human airway tree," *J. Appl. Physiol.*, vol. 87, pp. 2207–2217.
28. Finlay, W. (2019) *The Mechanics of Inhaled Pharmaceutical Aerosols*. Academic Press.
29. Nowak, N., Kakade, P. P., & Annapragada, A. V. (2003). Computational fluid dynamics simulation of airflow and aerosol deposition in human lungs. *Annals of biomedical engineering*, *31*(4), 374-390.
30. Gemci, T., Ponyavin, V., Chen, Y., Chen, H., & Collins, R. (2008). Computational model of airflow in upper 17 generations of human respiratory tract. *Journal of Biomechanics*, *41*(9), 2047-2054.
31. Walters, D. K., & Luke, W. H. (2010). A method for three-dimensional Navier–Stokes simulations of large-scale regions of the human lung airway. *Journal of Fluids Engineering*, *132*(5).
32. Fernández-Tena, A. (2014) "Clinical applications of fluid dynamics models in respiratory diesase", University of Oviedo, Spain.

http://digibuo.uniovi.es/dspace/bitstream/10651/29057/6/TD_AnaFernandezTena.pdf
33. Tena, A. F., Fernández, J., Álvarez, E., Casan, P., & Walters, D. K. (2017). Design of a numerical model of lung by means of a special boundary condition in the truncated branches. *International journal for numerical methods in biomedical engineering*, *33*(6), e2830.
34. Pandal-Blanco, A., Barrio-Perotti, R., Agujetas-Ortiz, R., & Fernández-Tena, A. (2019). Implementation of a specific boundary condition for a simplified symmetric single-path CFD lung model with OpenFOAM. *Biomechanics and modeling in mechanobiology*, *18*(6), 1759-1771.
35. Fernández-Tena, A., Barrio-Perotti, R., Blanco-Marigorta, E., & Pandal-Blanco, A. (2020). In silico prototype of a human lung with a single airway to predict particle deposition. *International Journal for Numerical Methods in Biomedical Engineering*. doi:10.1002/cnm.3339
36. Ley, S., Mayer, D., Brook, B., van Beek, E., Heussel, C., Rinck, D., ... & Kauczor, H. U. (2002). Radiological imaging as the basis for a simulation software of ventilation in the tracheo-bronchial tree. *European radiology*, *12*(9), 2218-2228.
37. Schmidt, A., Zidowitz, S., Kriete, A., Denhard, T., Krass, S., & Peitgen, H. O. (2004). A digital reference model of the human bronchial tree. *Computerized Medical Imaging and Graphics*, *28*(4), 203-211.
38. Cebral, J. R., & Summers, R. M. (2004). Tracheal and central bronchial aerodynamics using virtual bronchoscopy and computational fluid dynamics. *IEEE transactions on medical imaging*, *23*(8), 1021-1033.
39. Nakamura, M., Wada, S., Miki, T., Shimada, Y., Suda, Y., & Tamura, G. (2008). Automated Segmentation and Morphometric Analysis of the Human Airway Tree from Multi-Detector CT Images. *The Journal of Physiological Sciences*, 0812050088-0812050088.
40. Gore, J. C. (2020) "Artificial intelligence in medical imaging," *Magn. Reson. Imaging*, vol. 68.
41. Pourmehran, O., Gorji, T. B., & Gorji-Bandpy, M. (2016). Magnetic drug targeting through a realistic model of human tracheobronchial airways using computational fluid and particle dynamics. *Biomechanics and modeling in mechanobiology*, *15*(5), 1355-1374.
42. Yousefi, M., Pourmehran, O., Gorji-Bandpy, M., Inthavong, K., Yeo, L., & Tu, J. (2017). CFD simulation of aerosol delivery to a human lung via surface acoustic wave nebulization. *Biomechanics and modeling in mechanobiology*, *16*(6), 2035-2050.
43. Darquenne, C., Fleming, J. S., Katz, I., Martin, A. R., Schroeter, J., Usmani, O. S., ... & Schmid, O. (2016). Bridging the gap between science and clinical efficacy: physiology, imaging, and modeling of aerosols in the lung. *Journal of aerosol medicine and pulmonary drug delivery*, *29*(2), 107-126.
44. Bos, A. C., Van Holsbeke, C., De Backer, J. W., van Westreenen, M., Janssens, H. M., Vos, W. G., & Tiddens, H. A. (2015). Patient-specific modeling of regional antibiotic concentration levels in airways of patients with cystic fibrosis: Are we dosing high enough? *PLoS One*, *10*(3).
45. Jiang, F., Hirano, T., Ohgi, J., & Chen, X. (2020). A voxel image-based pulmonary airflow simulation method with an automatic detection algorithm for airway outlets. *International Journal for Numerical Methods in Biomedical Engineering*, e3305.

46. Poorbahrami, K., & Oakes, J. M. (2019). Regional flow and deposition variability in adult female lungs: A numerical simulation pilot study. *Clinical Biomechanics*, *66*, 40-49.
47. Lizal, F., Jedelsky, J., Morgan, K., Bauer, K., Llop, J., Cossio, U., ... & Koch, E. (2018). Experimental methods for flow and aerosol measurements in human airways and their replicas. *European Journal of Pharmaceutical Sciences*, *113*, 95-131.
48. Islam, M. S., Saha, S. C., Sauret, E., Gemci, T., & Gu, Y. (2017). Pulmonary aerosol transport and deposition analysis in upper 17 generations of the human respiratory tract. *Journal of Aerosol Science*, *108*, 29-43.
49. Lin, C. L., Tawhai, M. H., McesLennan, G., & Hoffman, E. A. (2009). Multiscale simulation of gas flow in subject-specific models of the human lung. *IEEE Eng. Med. Biol. Mag*, *28*(3), 25-33.
50. Lin, C. L., Tawhai, M. H., & Hoffman, E. A. (2013). Multiscale image-based modeling and simulation of gas flow and particle transport in the human lungs. *Wiley Interdisciplinary Reviews: Systems Biology and Medicine*, *5*(5), 643-655.
51. Roth, C. J., Ismail, M., Yoshihara, L., & Wall, W. A. (2017). A comprehensive computational human lung model incorporating inter-acinar dependencies: Application to spontaneous breathing and mechanical ventilation. *International journal for numerical methods in biomedical engineering*, *33*(1), e02787.
52. Tawhai, M. H., Hunter, P., Tschirren, J., Reinhardt, J., McLennan, G., & Hoffman, E. A. (2004). CT-based geometry analysis and finite element models of the human and ovine bronchial tree. *Journal of applied physiology*, *97*(6), 2310-2321.
53. Andersson, A. G., Hellström, J. G. I., Andreasson, P., & Staffan Lundström, T. (2014). Effect of spatial resolution of rough surfaces on numerically computed flow fields with application to hydraulic engineering. *Engineering Applications of Computational Fluid Mechanics*, *8*(3), 373-381.
54. Fernández-Tena A, Marcos AC, Agujetas R, Ferrera C. (2018). Simulation of the human airways using virtual topology tools and meshing optimization. Biomechanics and Modeling in Mechanobiology. 17(2): 465–477.
55. ANSYS Version 18.2 (2017) ©ANSYS Inc.
56. Hounsfield, GN (1973) Computerized transverse axial scanning (tomography): part I. Description of system. Br J Radiol 46:1016–1022.
57. 3D Slicer V4.4.0 (2014). https://www.slicer.org.
58. Fedorov, A., Beichel, R., Kalpathy-Cramer, J., Finet, J., Fillion-Robin, J. C., Pujol, S., ... & Buatti, J. (2012). 3D Slicer as an image computing platform for the Quantitative Imaging Network. Magnetic resonance imaging, 30(9), 1323-1341.
59. Janna, W. S. (2015). Introduction to fluid mechanics. CRC press.
60. Menter, F. (2018). "Stress-Blended Eddy Simulation (SBES)— A New Paradigm in Hybrid RANS-LES Modeling," in Progress in Hybrid RANS-LES Modelling. HRLM2016. Notes on Numerical Fluid Mechanics and Multidisciplinary Design, 137, Springer, pp. 27–38.
61. Wilcox, D. C. (2008) "Formulation of the k-ω turbulence model revisited," AIAA J., vol. 46, no. 11, pp. 2823–2838.
62. Xu, X., Wu, J., Weng, W. et al. (2020). Investigation of inhalation and exhalation flow pattern in a realistic human upper airway model by PIV experiments and CFD simulations. Biomech Model Mechanobiol. https://doi.org/10.1007/s10237-020-01299-3.
63. Zhang, Z., & Kleinstreuer, C. (2011). Laminar-to-turbulent fluid–nanoparticle dynamics simulations: Model comparisons and nanoparticle-deposition applications.

International Journal for Numerical Methods in Biomedical Engineering, *27*(12), 1930-1950.

64. Fernández-Tena, A., Marcos, A. C., Martínez, C., & Keith Walters, D. (2017). A new adaptive time step method for unsteady flow simulations in a human lung. Computer methods in biomechanics and biomedical engineering, 20(8), 915-917.